# Swimming in Circles: Motion of Bacteria near Solid Boundaries

Eric Lauga,* Willow R. DiLuzio,*† George M. Whitesides,† and Howard A. Stone*
*Division of Engineering and Applied Sciences, and †Department of Chemistry and Chemical Biology, Harvard University, Cambridge, Massachusetts

ABSTRACT   Near a solid boundary, *Escherichia coli* swims in clockwise circular motion. We provide a hydrodynamic model for this behavior. We show that circular trajectories are natural consequences of force-free and torque-free swimming and the hydrodynamic interactions with the boundary, which also leads to a hydrodynamic trapping of the cells close to the surface. We compare the results of the model with experimental data and obtain reasonable agreement. In particular, the radius of curvature of the trajectory is observed to increase with the length of the bacterium body.

## INTRODUCTION

The bacterium *Escherichia coli* (*E. coli*) has been a microorganism of choice for studying a variety of biological and biomechanical processes. In particular, *E. coli* has been used as the prototypical micro-swimmer (1,2). In solution, *E. coli* cells swim in a random walk, with approximately straight swimming trajectories alternating with rapid reorientations. When *E. coli* cells are close to a surface, however, they trace out clockwise (when viewed from above the surface) circular trajectories (3–8), and are observed to stay near the surface for long periods of time (8), enhancing the probability of their adhesion to the substrate. Consequently, the motility of *E. coli* near surfaces is important in the early stages of biofilm formation and pathogenic infection (9,10). In this article, we provide a hydrodynamic model for such circular motion.

*E. coli* and other peritrichously flagellated bacteria swim by the action of rotary motors (usually two to six) embedded in the cell wall (2). The motors rotate counter-clockwise or clockwise, when viewed from behind the cell, with each motor driving a long, thin, left-handed helical flagellar filament. If all the motors rotate counter-clockwise in a viscous fluid (e.g., water), the flagella bundle together and propel the bacterial cell forward. This motion is called a ''run''. If one or more motors rotate clockwise, the flagella unbundle, and the bacteria tumbles. The forward thrust generated by the flagellar bundle during a run is opposed by the translational viscous drag on the entire cell. Each flagellum (average length, $\sim$7 $\mu$m) rotates at speeds of $\sim$100 Hz (11,12) and its counter-clockwise rotation exerts a net torque on the cell body (average length, 2–5 $\mu$m). To balance this torque, the cell body counter-rotates in a clockwise direction (viewed from behind the organism) at speeds of $\sim$10 Hz (13).

As described above, *E. coli* cells near solid surfaces do not have straight runs but are observed to trace out clockwise circles. An early observation of this circular motion (1971),

reported in Berg and Turner (4), measured a radius of curvature for the circles on the order of 25 $\mu$m. The swimming direction was clockwise when viewed from above, which the authors expected, as the flagellar bundle rotates counterclockwise and the cell body rotates clockwise. The influence of temperature on the motility of *E. coli* was considered in Maeda et al. (3); this work reported circular curves for the motion near a glass slide, with a radius on the order of 10–50 $\mu$m, and which increased with temperature. A tracking microscope was used later (5,6) to follow the trajectory of *E. coli* near a glass surface. Again, near solid boundaries, the bacteria were observed to swim in circles, with radius of $\sim$13 $\mu$m; the authors also found that the swimming speed increased with the distance from the boundary. The question of attraction between the swimming bacteria and solid surface has been studied in Vigeant and Ford (7) and Vigeant et al. (8), and the distance to the surface has been measured (tens of nanometers). It was found that standard Derjaguin-Landau-Verwey-Overbeek theory could not explain the tendency of the cells to stay near the surfaces, but that some other force was still to be identified. The authors proposed that, because of their nonspherical shape, the cells swim at an angle to the surface, and therefore constantly swim into the surface. More recently, a related study on the motion of *Vibrio alginolyticus* near surfaces has reported circular trajectories as well (14,15).

Numerically, there has been only one study that has considered the hydrodynamics of a swimming bacteria near a no-slip surface (16) (see also early work on flagellar motion near boundaries in (17–21)). The bacterium was modeled as a body of spherical shape with a single, solid, helical flagellum and the boundary integral method was used for the numerical investigation. In this approach, the total flow field was given by a distribution of fundamental singularities for Stokes flow along the surface of the microorganism. In the simulations, circular motion was obtained with a radius of curvature on the order of the length of the microorganism ($\sim$10 $\mu$m), with a tendency for the microorganism to swim toward the wall and crash into it. Furthermore, the authors proposed a

physical picture for a clockwise motion. However, no simple analytical model was proposed and a numerical integration was required to obtain the cell trajectories.

The goal of this article is to provide a hydrodynamic model for the motion of *E. coli* near solid boundaries. We first summarize our experiments to obtain a new set of data on swimming speed and circular trajectories for *E. coli* strain HCB437 near solid surfaces. We then present our geometrical model for *E. coli*, and the physical picture for the circular trajectory of the bacterium near a no-slip surface, based on the change in hydrodynamic resistance of elements along the cell body due to the nearby surface. Using resistive-force theory, we calculate the trajectory of the bacterium. Since the full model requires a matrix inversion to be evaluated, we also present an approximate analytical solution for the trajectory. In particular, we show that the circular motion is clockwise when viewed from above the surface, and that the cells need to swim into the surface as a natural consequence of force-free and torque-free swimming. We then illustrate the results of our two models (the full model and its analytical approximation), show their dependence on various geometrical parameters of the cell, and compare the models with our experiments. We find that our models are consistent with experimental swimming speeds and radii of curvature of the circular motions, and that they allow us to obtain an estimate for the relation between the size of the bacterium and its distance to the surface. The values of the various hydrodynamic mobilities used in the model are presented in Appendix A, and the cell trajectory far from a surface is given in Appendix B.

## EXPERIMENT

We examined a dilute suspension of smooth-swimming (i.e., non-tumbling) *E. coli* cells (HCB437) (22) in an observation chamber. The cells were observed from outside the chamber above the surface, swimming with counter-clockwise trajectories; consequently, when viewed from within the liquid (what we will refer to as ''above the surface'' in the remainder of the article), they are performing clockwise trajectories. In Fig. 1, we provide superimposed video images showing the curved trajectories that cells follow when swimming near the glass surface.

## Materials and methods

### Preparation of motile cells

*E. coli* strain HCB437 (22) used in these studies is a smooth-swimming strain that is deleted for most chemotaxis genes. During cell growth, cells double their length and then divide at their approximate midpoint (septate), while maintaining a constant width. The length of cells naturally vary depending on the progress of cells through the growth cycle (23). Media components were purchased from Difco (Tucker,
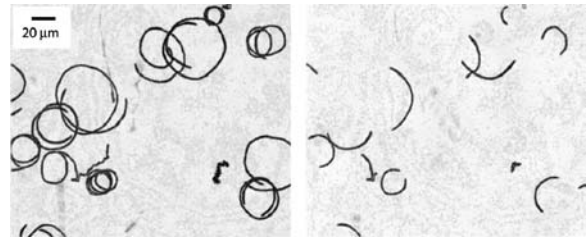


FIGURE 1 Superimposed phase-contrast video microscopy images show *E. coli* cells (HCB437) swimming in circular trajectories near a glass surface. (*Left*) Superposition of 8 s (240 frames) of video images. (*Right*) Typical superposition of 2 s (60 frames) of video images that was used to analyze the length and width of cells, the swimming speed of cells, and the radius of curvature of the trajectories.

GA) or Sigma (St. Louis, MO). Saturated *E. coli* cultures were grown for 16 h in tryptone broth (1% tryptone and 0.5% NaCl) using a rotary shaker (200 rpm) at 33°C. Saturated cultures were frozen at −70°C in 15% glycerol. Motile *E. coli* cultures were obtained by diluting 50 μL of the thawed saturated culture into 5 mL of fresh tryptone broth, and grown in 14 mL sterile, polypropylene tubes at 33°C on a rotary shaker (150 rpm) for 3.5 h. Cells were washed by three successive centrifugations at 2000 *g* for 8 min and were resuspended into motility buffer (24) (1 mM potassium phosphate, pH 7.0, 0.1 mM Na-EDTA) containing 10 mM glucose and 0.18% (w/v) methylcellulose (Methocel 90; Biochemika, Fluka, St. Louis, MO). Glucose was added to maintain motility in an anaerobic environment and methylcellulose was added to reduce the tendency of cells to wobble (25) (solutions of methylcellulose are Newtonian at concentrations <0.5% (26)). Filamentous cells were obtained by growing motile cells for 3.5 h as described above, adding 50 μg/mL cephalexin to the culture, and then growing cells an additional 0.5 h (27). Filamentous cells were then washed as described above.

### Observation of swimming cells

A volume of 50 μL of the washed cell suspension (~$10^6$ cells/mL) was added to an observation chamber constructed from two glass coverslips and double-sided tape (Scotch, permanent; 3M, St. Paul, MN). The chamber dimensions were ~1-cm wide, ~2-cm long, and ~80-μm high. The microscope coverslips were alternately rinsed with soap and DI water, DI water, ethanol, DI water, and then treated with an air plasma for 1 min at 1–2 Torr (SPI Plasma Prep II; Structure Probes/SPI Supplies, West Chester, PA). The observation chamber was heated to 32°C using a heated microscope stage (Research Instruments, Singapore). Cells swimming near the upper glass coverslip were observed using a Nikon Eclipse E400 upright, phase-contrast microscope (Nikon, Marunouchi, Tokyo). Video images were acquired using a 20× or 40× Nikon phase objective and a monochrome CCD camera (Model No. V1070; Marshall Electronics, El Segundo, CA) connected to a digital video

recorder (Model No. GV-D1000, Sony, San Diego, CA) that collected 640 pixel × 480 pixel images at 30 frames per second.

### Image analysis

Video was captured into a computer using Adobe Premiere (Adobe, San Jose, CA) and analyzed using ImageJ (available for download at http://rsbweb.nih.gov/ij/) or Scion Image (available for download at http://www.scioncorp.com) using standard analysis tools. Video images were thresholded so that cells appeared black and the background appeared white. The following parameters were measured for individual cells in 60 consecutive video frames (2 s): The projected area of the cell, the midpoint of the cell, and the short and long axis of the cell (approximating the cell shape as an ellipse). The average of these values measured over the 2-s interval was used. The average cell speed was calculated by measuring the average distance that the midpoint of the cell traveled between each video frame and dividing this distance by the video collection rate (30 fps or 0.033 s). The radius of curvature of the cell trajectory was calculated by making a least-square fit of a circle to the 2-s trajectory of the midpoint of the cell. A small amount of error was introduced by the collection and analysis of cells from multiple regions of the swimming chambers and from multiple chambers. Small changes in focus and lighting in different regions led to variability in the thresholding, which led to some error in the measurement of cell widths and lengths. The error due to differences in focus and lighting were <10%, as judged by the variability in the widths of cell. We minimized these effects by using the measured aspect ratio of cells and an average value (1.5 $\mu$m) for the width of cells in all calculations below.

### Results

In Fig. 2 we plot the experimental results for the cell swimming speed ($U$) and the radius of curvature of the circles ($\mathcal{R}$) as a function of the equivalent sphere radius, $a$, that is, the radius of the sphere that has the same viscous resistance as the prolate ellipsoid of measured cell width and aspect ratio, translating along its axis of symmetry (28),
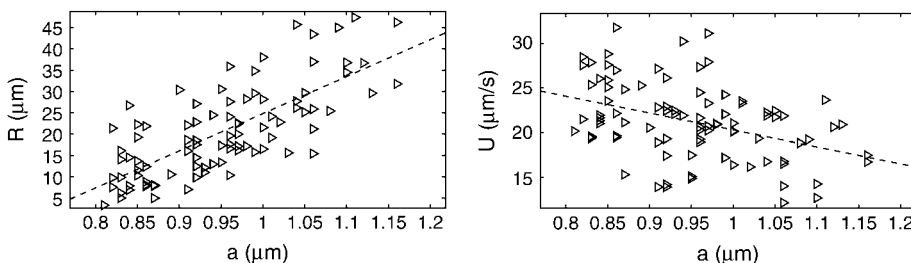
$$\frac{a}{w} = \frac{4}{3} \frac{1}{\frac{2\phi^2 - 1}{(\phi^2 - 1)^{3/2}} \ln\left(\frac{\phi + \sqrt{\phi^2 - 1}}{\phi - \sqrt{\phi^2 - 1}}\right) - \frac{2\phi}{\phi^2 - 1}}, \quad (1)$$

where $w$ is the width of the cell and $\phi$ its aspect ratio (see Table 1 for a summary of the symbols used in the article). As explained above, we take $w$ to be the average of the measured cell widths to minimize focus and lighting differences ($w = 1.5 \mu$m) and measure the value of $\phi$. The scatter in the experimental data, evident in Figs. 1 and 2, can be explained by the natural cell-to-cell variability in the number of flagella (29), flagellar length, flagellar rotation rates (12), and distances of cells from the surface (8) (parameters that might also be function of cell length); we address the effects that these parameters have on the predicted radius of curvature below. Nonetheless, the experimental data demonstrate a statistically significant ($R^2 = 0.55$) increase of the radius of curvature of the trajectories of cells swimming near a glass surface with the cell size.

## MODEL

We present in this section our hydrodynamic model for the motion of *E. coli* near a flat no-slip surface and give a simple physical picture for the circular trajectory.

### Setup

We model the bacterium as a single, left-handed rigid helix attached to a spherical body (16,30,31) of radius $a$ whose center of mass is located at a distance $d$ above a solid surface, as illustrated in Fig. 3; the liquid gap between the solid surface and the cell body has height $h$. At the concentration we use, cells are separated by at least one body length, i.e., approximately 10 $\mu$m. Force-free flows, as the flow around a swimming bacteria, decay spatially at least as fast as $1/r^2$, where $r$ is the distance from the cell, and possibly faster when near solid boundaries, and as a consequence, cells are not expected to interact hydrodynamically with each other. The cell is assumed to be parallel to the surface and oriented in the $y$ direction. The helix is assumed to have thickness $2r$, radius $b$, wavelength $\lambda$, with a number $n$ of wavelengths along the helix, such that the total length of the helix along



FIGURE 2 Results of our experimental investigation of swimming *E. coli* near solid boundaries. (*Left*) Radius of curvature of the circular trajectory, $\mathcal{R}$, as a function of the equivalent sphere radius, $a$, of the elliptical cell body (see text). (*Right*) Swimming speed, $U$, versus equivalent body radius, $a$. In both cases, we have added as dashed lines the best least-square fit to the data of the form $\alpha a + \beta$. (*Left*) $\alpha = 86.78$, $\beta = -61.99$ $\mu$m, and $R^2 = 0.55$. (*Right*) $\alpha = -19.09$ s$^{-1}$, $\beta = 39.39$ $\mu$m s$^{-1}$, and $R^2 = 0.165$.

**TABLE 1 List of symbols used in this article and their meaning**

| Symbol | Meaning |
|---|---|
| $\mathbf{U}$ | Velocity of the cell, $\mathbf{U} = (U_x, U_y, U_z)$. |
| $\mathbf{\Omega}$ | Rotation rate of the cell, $\mathbf{\Omega} = (\Omega_x, \Omega_y, \Omega_z)$. |
| $U$ | Planar swimming velocity of the bacteria, $U = \left(U_x^2 + U_y^2\right)^{1/2}$. |
| $\mathcal{R}$ | Radius of curvature of the trajectory, $\mathcal{R} = U/|\Omega_z|$. |
| $a$ | Equivalent sphere radius, given by Eq. 1. |
| $w, \phi$ | Width and aspect ratio of the cell. |
| $d$ | Distance between the center of the cell and the surface. |
| $h$ | Gap thickness between the cell and the surface. |
| $r$ | Radius of the flagella filament (bundle). |
| $b, \lambda$ | Radius and wavelength of the helix. |
| $n$ | Number of wavelength in the flagella. |
| $L_\parallel$ | Length of the flagella $L_\parallel = n\lambda$. |
| $\omega$ | Rotation rate of the flagella (in the frame attached to the cell body). |
| $\mathcal{F}_x^1, \mathcal{F}_x^2$ | Local forces responsible for the cell rotation near the surface (see Fig. 4). |
| $\boldsymbol{\mathcal{F}}$ | $\boldsymbol{\mathcal{F}} = (\mathcal{F}_x, \mathcal{F}_y, \mathcal{F}_z)$. |
| $\boldsymbol{\mathcal{L}}$ | $\boldsymbol{\mathcal{L}} = (\mathcal{L}_x, \mathcal{L}_y, \mathcal{L}_z)$. |
| $\mathcal{M}, \mathcal{W}$ | Mobilities of the cell body; $\mathcal{M}$ ($\mathcal{W}$) is non-zero (zero) away from the surface. |
| $\mathcal{N}, \mathcal{V}$ | Mobilities of the flagella; $\mathcal{N}$ ($\mathcal{V}$) is non-zero (zero) away from the surface. |
| $\mathcal{M}_{ij}^{\alpha\beta}$ | Typical notation for the viscous mobilities, $\mathcal{M}_{ij}^{\alpha\beta} = \partial\alpha_i/\partial\beta_j$. |
| $\alpha$ | Either $F$, for force, or $L$, for torque. |
| $\beta$ | Either $U$, for velocity, or $\Omega$, for rotation rate. |
| $c_\parallel, c_\perp$ | Local drag coefficient for motion parallel and perpendicular to local length. |
| $\mathbf{u}_\parallel, \mathbf{u}_\perp$ | Component of local velocity parallel and perpendicular to local length. |
| $\mu$ | Shear viscosity of the liquid. |
| $\overline{c_\parallel}$ | Value of $c_\parallel$ at a distance $d$ to the surface. |
| $f(z)$ | Variation of $c_\parallel$ from $\overline{c_\parallel}$, that is $f(z) = c_\parallel/\overline{c_\parallel}$. |
| $\mathcal{A}, \mathcal{B}$ | Mobility matrix for the cell body and the helical flagellar bundle. |
| $h_0, a_1, a_2$ | Parameters for the linear increase of $h$ with $a$ (Eq. 25). |
| $\epsilon$ | Slenderness of the helical flagella, $\epsilon = 2\pi b/\lambda$. |
| $s$ | Curvilinear coordinate along the flagella. |
| $\mathcal{I}, \mathcal{J}$ | Integrals involved in the flagellar mobility calculations (Eq. 29). |



FIGURE 3 Setup and notations for the mechanical model of *E. coli* swimming near a solid surface.

the $y$ direction is $L_\parallel = n\lambda$. The assumption of sphericity, although not completely realistic for the cell body of *E. coli* which is more like a 2:1 prolate ellipsoid, was made in order to use well-known mobility formulae, and we expect therefore our results to be correct within a shape factor of order unity. Due to the action of rotary motors, the bundle is rotating in the counter-clockwise direction (viewed from behind) with an angular velocity $\boldsymbol{\omega} = -\omega \, \mathbf{e}_y$ relative to the body, with $\omega > 0$ (see Fig. 3). We denote by $\mathbf{U} = (U_x, U_y, U_z)$ and $\mathbf{\Omega} = (\Omega_x, \Omega_y, \Omega_z)$ the instantaneous velocity and rotation rate (measured from the center of the cell body), respectively, of the bacterium.

## Physical picture

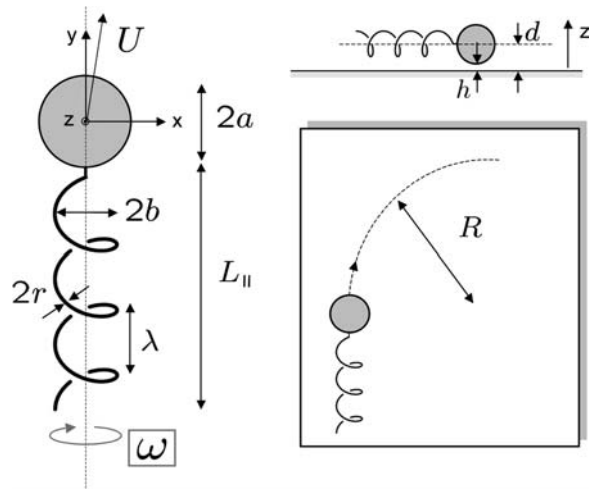In the absence of a nearby wall, the bacterium swims in a straight line, $\mathbf{U} = U_y \, \mathbf{e}_y$, and rotates along its swimming axis, $\mathbf{\Omega} = \Omega_y \, \mathbf{e}_y$. The velocity $U_y > 0$ is obtained by balancing the propulsive force of the helical bundle with the viscous resistance on the whole bacterium and the rotation rate $\Omega_y > 0$ is found by the balance of viscous moments around the $y$ axis (see Appendix B).

What changes when the microorganism is swimming near a solid surface? Both the cell body and the helical bundle contribute together to a rotation of the bacterium around the $z$ axis (see notations in Fig. 3; see also (32)).

First, as the cell body is near the surface, when it rotates around the $y$-axis at a rate $\Omega_y > 0$, there is a viscous force acting on the cell body in the $x$-direction, $\mathcal{F}_x^1 \, \mathbf{e}_x$, with $\mathcal{F}_x^1 > 0$ (see diagram on Fig. 4 *a*). This is a standard hydrodynamic result (28) and an intuitive way to think about this result is to picture a ball in a liquid film near a surface; pushing the ball along the surface will also make it rotate, and vice versa.

The bundle of flagella is also acted upon by a net force in the $x$-direction, induced by the presence of the wall. Since the bundle takes the shape of a helix, parts of the bundle are located close to the surface and parts are located further away (see Fig. 4). The local drag coefficient on an elongated filament decreases with increasing distance from the nearby surface (see details below), which means that the parts of the bundle that are close to the surface will be subjected to a larger local viscous force compared to portions of the helix located further away from the surface. As the helical bundle rotates counter-clockwise around the $y$ axis (viewed from behind), the portions of the helix that are closer to the surface have a positive $x$ velocity, and therefore the net viscous force acting on the bundle, $\mathcal{F}_x^2 \, \mathbf{e}_x$, is negative, $\mathcal{F}_x^2 < 0$ (see diagram in Fig. 4 *b*). Note that since the swimming bacterium as a whole is force-free, we have necessarily $\mathcal{F}_x^2 = -\mathcal{F}_x^1$.

As a consequence of the viscous forces acting on both the helical bundle and the cell body and their spatial distribution,
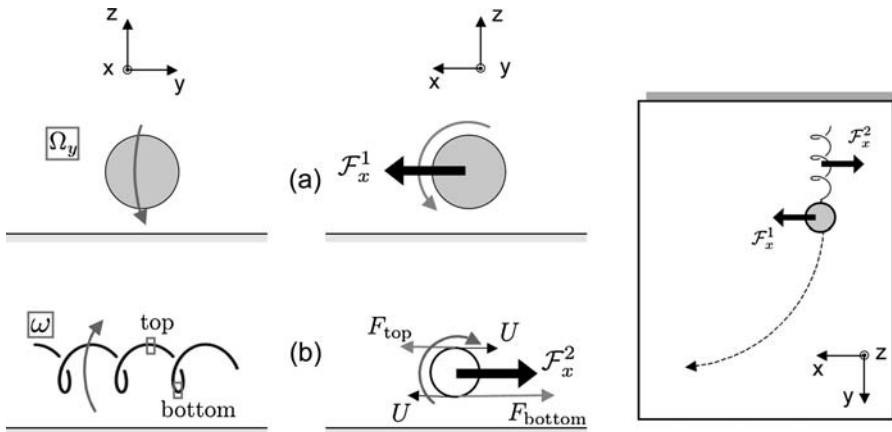
FIGURE 4 Physical picture (*side* and *front views*) for the out-of-plane rotation of the bacterium: (*a*) The positive *y*-rotation of the cell body leads to a net viscous *x*-force on the cell body, $\mathcal{F}_x^1 > 0$. (*b*) The negative *y*-rotation of the helical bundle leads to a net negative viscous *x*-force on the flagella, $\mathcal{F}_x^2 < 0$. The spatial distribution of these forces leads to a negative *z*-torque on the bacterium, which makes it rotate clockwise around the *z*-axis. Therefore, when viewed from above, the bacterium swims to its right.

a negative torque, $\mathcal{L}_z < 0$, will act on the bacterium and will rotate the entire cell clockwise around the *z* axis (Fig. 4, *right*). When viewed from above, the bacterium will therefore swim to the right, as is observed experimentally. Since the bacterium as a whole is torque-free (the inertia of the organism is much smaller than the resisting fluid forces, so forces and torques on the organism need to balance at each instant), this torque will be balanced by a positive torque arising from the viscous resistance to a rotation around the *z* axis.

This physical picture allows us to obtain an estimate for the radius of curvature $\mathcal{R}$ of the motion, as the ratio of the swimming velocity $U_y$ to the out-of-plane rotation rate $\Omega_z$. Since the Reynolds number for the flow number is low (typically $Re \approx 10^{-4}$), the equations of motion for the fluid are linear (Stokes flow), and therefore instantaneous viscous forces and torques for various parts of the bacterium are linearly related to their velocities and rotation rates, with linear coefficients usually termed mobilities (see Eqs. 8 and 9 below).

We denote by $\mathcal{M}$ and $\mathcal{N}$ the viscous mobilities of the bacterium flagella and body, respectively, which are non-zero even in the absence of a wall, and by $\mathcal{W}$ and $\mathcal{V}$ those which are equal to zero when the microorganism swims far from the surface. For example, the mobility relating the *y* component of the viscous force to the *y* component of the cell velocity will be denoted by an $\mathcal{M}$-symbol, as it is non-zero even without the presence of the nearby surface, but the mobility relating the *x* component of the viscous torque to the *y* component of the cell velocity will be denoted by a $\mathcal{W}$-symbol, as this mobility is equal to zero far away from a solid boundary. This distinction will allow us to get a clear understanding of the physical mechanisms at play when we obtain formulae for the motion of the organism.

For all these mobilities (say $\mathcal{M}$ for illustration purposes) we will use notations of the form $\mathcal{M}_{ij}^{\alpha\beta}$, where the superscript $\alpha\beta$ is either $FU$, in which case $\mathcal{M}_{ij}^{FU}$ denotes how the $i^{th}$ component of a viscous force is linearly related to the $j^{th}$ component of the cell velocity ($F_i = \mathcal{M}_{ij}^{FU} U_j$), $F\Omega$ (relation

between force and rotation rate), $LU$ (relation between torque and velocity), or $L\Omega$ (relation between torque and rotation rate). We will also always use the convention that the mobilities are positive, and will therefore appear with a minus sign when necessary (see Eqs. 8 and 9).

To have an estimate of the radius of curvature of the trajectories, we need to estimate both the swimming velocity and the out-of-plane rotation. The swimming velocity is obtained by balancing the propulsive force of the microorganism due to the rotation of the flagella, $\mathcal{M}_{yy}^{F\Omega}(\omega - \Omega_y)$, with the viscous drag on the whole bacterium, given by $(\mathcal{M}_{yy}^{FU} + \mathcal{N}_{yy}^{FU})U_y$, so that

$$\mathcal{M}_{yy}^{F\Omega}(\omega - \Omega_y) \approx (\mathcal{M}_{yy}^{FU} + \mathcal{N}_{yy}^{FU})U_y. \qquad (2)$$

The rotation rate can be estimated by balancing the wall-induced torque mentioned above, also due to rotation of the flagella, $\mathcal{L}_z \approx \mathcal{W}_{zy}^{L\Omega}(\omega - \Omega_y)$, with the viscous torque resisting rotation of the whole bacterium. This is mostly due to the viscous resistance of the long flagella, $-\mathcal{M}_{zz}^{L\Omega}\Omega_z$, which is

$$\mathcal{W}_{zy}^{L\Omega}(\omega - \Omega_y) \approx -\mathcal{M}_{zz}^{L\Omega}\Omega_z. \qquad (3)$$

By evaluating the ratio of the two previous balances, we obtain an estimate for the radius of the circular motion as

$$\mathcal{R} \approx \frac{U_y}{|\Omega_z|} \approx \frac{\mathcal{M}_{zz}^{L\Omega}\mathcal{M}_{yy}^{F\Omega}}{\mathcal{W}_{zy}^{L\Omega}(\mathcal{M}_{yy}^{FU} + \mathcal{N}_{yy}^{FU})}. \qquad (4)$$

Away from the surface, $\mathcal{W}_{zy}^{L\Omega}$ becomes small and therefore the radius of curvature of the trajectory will become large, which is expected as bacteria (during a run) swim in straight lines. (Note that both translational and rotational diffusion, neglected in this article, will actually prevent *E. coli* from swimming in a straight line for more than a few seconds.) As is demonstrated below, the simple estimate given by Eq. 4 is consistent with a more detailed calculation for the cell trajectory.

# TRAJECTORY CALCULATION FOR THE BACTERIUM

We proceed in this section by presenting the detailed calculation for the trajectory of the bacterium using resistive-force theory for the flagellar hydrodynamics, and exploit it to obtain an approximate analytical solution.

## Modeling of flagella hydrodynamics

The modeling chosen here for the helical hydrodynamics is that of resistive-force theory (RFT), as first introduced by Gray and Hancock (34), since it is the simplest approach to the zero-Reynolds-number hydrodynamics of elongated bodies. The method is an approximation to the equations of slender-body theory (SBT). SBT considers the zero-Reynolds-number dynamics of long and slender filaments by distributing fundamental Stokes flow singularities at their centerline (33,35). The idea was first introduced by Hancock (36), is reviewed in detail by Lighthill (37), and has been applied to the case of helical flagella in Higdon (30).

RFT is the leading-order approximation of SBT, which gives results accurate at order $\mathcal{O}([\log(L/r)]^{-1})$, where $L$ is the length along the filament and $r$ its radius. The complexity of fully solving for the spatial distribution of singularities on a moving flagellar filament is replaced by introducing a set of local drag coefficients. Let us consider a portion of the filament of length $\delta\ell$, oriented along the tangential vector, $\mathbf{t}$, and moving at a velocity $\mathbf{u}$ in a viscous liquid. The local velocity can be decomposed into a parallel and perpendicular components, $\mathbf{u} = \mathbf{u}_\parallel + \mathbf{u}_\perp$, where $\mathbf{u}_\parallel$ is parallel to the tangential vector, $\mathbf{u}_\parallel = (\mathbf{u} \cdot \mathbf{t})\mathbf{t}$, and $\mathbf{u}_\perp$ is perpendicular to it, $\mathbf{u}_\perp = \mathbf{u} - \mathbf{u}_\parallel$. RFT assigns values for the local drag coefficients, $c_\parallel$ and $c_\perp$, which relate the local viscous force per unit length to the local parallel and perpendicular velocities, such that the total force on an element of length $\delta\ell$ can be written

$$\delta\mathbf{F} = -\delta\ell(c_\parallel \mathbf{u}_\parallel + c_\perp \mathbf{u}_\perp). \qquad (5)$$

For a periodic flagellar filament (wavelength $\lambda$) performing planar oscillations in a liquid of viscosity $\mu$ and far from a solid surface, we have approximately (21,34)

$$c_\parallel = \frac{2\pi\mu}{\ln(2\lambda/r) - 1/2}, \quad c_\perp = 2\,c_\parallel. \qquad (6)$$

The case of helical flagella was first considered in this context in Chwang et al. (38). Note that the drag anisotropy between tangential and perpendicular motion is the fundamental origin of the flagellar propulsion of microorganisms (2,34,37). Although it is only an approximate method, RFT has been shown in the past to provide both qualitative and quantitative information about the locomotion of microorganisms (21,34,37,39,40).

The presence of a solid surface modifies the values of the resistance coefficients for both the cell body and its flagella (18–21,41–45). Elements of the helical flagella are located at a distance $d(z)$ ranging between $d - b$ and $d + b$ to the solid surface, which are both smaller than the helix wavelength $\lambda$, so that the viscous resistance to motion of the flagella is dominated by the interactions with the surface. Since $r \ll d \pm b$, we consider the far-field asymptotic results of Katz et al. (19) (see also the review in Brennen and Winet (21)) and use

$$c_\parallel(z) = \frac{2\pi\mu}{\ln(2d\,(z)/r)}, \quad c_\perp = 2\,c_\parallel. \qquad (7)$$

Deviations from 2 for the ratio $c_\perp/c_\parallel$ were discussed in this context by Katz and Blake (20). We will denote by $\overline{c_\parallel}$ the value of the drag coefficient, Eq. 7, when $d(z) = d$, and will denote deviations from this value by the function $f$, so that $c_\parallel(z) = \overline{c_\parallel}f(z)$.

## Mobilities

We consider separately the mobilities of the cell body and its flagella, neglecting therefore the hydrodynamic interactions between these two parts of the microorganism. Although this is an approximation, we expect it will contribute only to a small error in the final results as the presence of a nearby surface leads to spatially localized flow fields, decaying at least as fast as a Stokeslet-dipole ($\sim 1/r^2$).

As described earlier, we denote by $\mathcal{M}$ and $\mathcal{N}$ the mobilities that are non-zero even in the absence of a wall, and by $\mathcal{W}$ and $\mathcal{V}$ those which are equal to zero when the microorganism swims far from the surface (with the conventions that the mobilities are positive). The mobility matrix for the spherical cell can be written as

$$
\begin{pmatrix} \mathcal{F}_x \\ \mathcal{F}_y \\ \mathcal{F}_z \\ \mathcal{L}_x \\ \mathcal{L}_y \\ \mathcal{L}_z \end{pmatrix} = \underbrace{\begin{pmatrix} -\mathcal{N}_{xx}^{FU} & 0 & 0 & 0 & \mathcal{V}_{xy}^{F\Omega} & 0 \\ 0 & -\mathcal{N}_{yy}^{FU} & 0 & -\mathcal{V}_{yx}^{F\Omega} & 0 & 0 \\ 0 & 0 & -\mathcal{N}_{zz}^{FU} & 0 & 0 & 0 \\ 0 & -\mathcal{V}_{xy}^{LU} & 0 & -\mathcal{N}_{xx}^{L\Omega} & 0 & 0 \\ \mathcal{V}_{yx}^{LU} & 0 & 0 & 0 & -\mathcal{N}_{yy}^{L\Omega} & 0 \\ 0 & 0 & 0 & 0 & 0 & -\mathcal{N}_{zz}^{L\Omega} \end{pmatrix}}_{\mathcal{A}} \cdot \begin{pmatrix} U_x \\ U_y \\ U_z \\ \Omega_x \\ \Omega_y \\ \Omega_z \end{pmatrix}, \qquad (8)
$$

and that of the helical flagella as

$$
\begin{pmatrix} \mathcal{F}_x \\ \mathcal{F}_y \\ \mathcal{F}_z \\ \mathcal{L}_x \\ \mathcal{L}_y \\ \mathcal{L}_z \end{pmatrix} = \underbrace{\begin{pmatrix} -\mathcal{M}_{xx}^{FU} & \mathcal{W}_{xy}^{FU} & 0 & \mathcal{M}_{xx}^{F\Omega} & \mathcal{W}_{xy}^{F\Omega} & -\mathcal{M}_{xz}^{F\Omega} \\ \mathcal{W}_{yx}^{FU} & -\mathcal{M}_{yy}^{FU} & 0 & -\mathcal{W}_{yx}^{F\Omega} & -\mathcal{M}_{yy}^{F\Omega} & \mathcal{W}_{yz}^{F\Omega} \\ 0 & 0 & -\mathcal{M}_{zz}^{FU} & \mathcal{M}_{zx}^{F\Omega} & 0 & \mathcal{M}_{zz}^{F\Omega} \\ \mathcal{M}_{xx}^{LU} & -\mathcal{W}_{xy}^{LU} & \mathcal{M}_{xz}^{LU} & -\mathcal{M}_{xx}^{L\Omega} & -\mathcal{W}_{xy}^{L\Omega} & 0 \\ \mathcal{W}_{yx}^{LU} & \mathcal{M}_{yy}^{LU} & 0 & -\mathcal{W}_{yx}^{L\Omega} & -\mathcal{M}_{yy}^{L\Omega} & \mathcal{W}_{yz}^{L\Omega} \\ -\mathcal{M}_{zx}^{LU} & \mathcal{W}_{zy}^{LU} & \mathcal{M}_{zz}^{LU} & 0 & \mathcal{W}_{zy}^{L\Omega} & -\mathcal{M}_{zz}^{L\Omega} \end{pmatrix}}_{\mathcal{B}} \cdot \begin{pmatrix} U_x \\ U_y \\ U_z \\ \Omega_x \\ \Omega_y - \omega \\ \Omega_z \end{pmatrix}, \tag{9}
$$

with values calculated in Appendix A. As can be seen in Eq. 9, the matrix $\mathcal{B}$ is almost full; the elements reported to be zero are either exactly zero at all instants or time-average to zero over the rotation period of a flagellar filament, $T = 2\pi/\omega$. If we define

$$
\mathcal{X} = (U_x, U_y, U_z, \Omega_x, \Omega_y, \Omega_z)^T, \quad \text{and} \quad \mathcal{Y} = (0, 0, 0, 0, \omega, 0)^T, \tag{10}
$$

then the requirement that the microorganism is free-swimming, $\mathcal{L} = 0$ and $\mathcal{F} = 0$, becomes a $6 \times 6$ linear system to solve for $\mathcal{X}$ of the form

$$
(\mathcal{A} + \mathcal{B})\mathcal{X} = \mathcal{B}\mathcal{Y}. \tag{11}
$$

The solution for the velocity, $\mathbf{U}$, and the rotation rate, $\mathbf{\Omega}$, can be found by simply substituting the values of the mobilities from Appendix A and numerically solving the linear system Eq. 11. The radius of curvature of the in-plane motion will then be given by

$$
\mathcal{R} = \frac{U}{|\Omega_z|}, \quad U = (U_x^2 + U_y^2)^{1/2}. \tag{12}
$$

## Approximate analytical solution

When the bacteria swims far from the solid surface, an analytical solution to motion can be found and we give it in Appendix B. In the presence of a solid surface, an analytical solution to the linear system, Eq. 11, exists in theory by direct matrix inversion, but it is very complicated and not very enlightening. We present below instead an approximate analytical solution of the linear system.

First, we note that, in the case of *E. coli*, a number of mobilities can be neglected between the elements of $\mathcal{A}$ and $\mathcal{B}$. They are

$$
\mathcal{N}_{zz}^{L\Omega} \ll \mathcal{M}_{zz}^{L\Omega}, \; \mathcal{N}_{xx}^{L\Omega} \ll \mathcal{M}_{xx}^{L\Omega}, \tag{13a}
$$

$$
\mathcal{M}_{zz}^{FU} \ll \mathcal{N}_{zz}^{FU}, \; \mathcal{M}_{yy}^{L\Omega} \ll \mathcal{N}_{yy}^{L\Omega}, \tag{13b}
$$

$$
\mathcal{W}_{xy}^{LU} \ll \mathcal{V}_{xy}^{LU}, \; \mathcal{W}_{yx}^{LU} \ll \mathcal{V}_{yx}^{LU}, \tag{13c}
$$

$$
\mathcal{W}_{xy}^{F\Omega} \ll \mathcal{V}_{xy}^{F\Omega}, \; \mathcal{W}_{yx}^{F\Omega} \ll \mathcal{V}_{yx}^{F\Omega}. \tag{13d}
$$

Furthermore, since the $x$ and $z$ components of both velocity and rotation rate are zero far from the solid surface, we make the assumption that, near the surface, these components

are at most on the order of the $y$ components: we therefore assume that $(U_x, U_z) \lesssim U_y$ and $(\Omega_x, \Omega_z) \lesssim \Omega_y$. We further assume that $\Omega_y \ll \omega$, as is the case far from the surface. Finally, since we have in general $(\mathcal{W}_{ij}^{\alpha\beta}, \mathcal{V}_{ij}^{\alpha\beta}) \ll (\mathcal{M}_{iy}^{\alpha\beta}, \mathcal{N}_{iy}^{\alpha\beta})$, where $j = x$ or $z$, these assumptions allow us to simplify further the mobilities in the matrices $\mathcal{A}$ and $\mathcal{B}$.

In that case, the equations $\sum \mathcal{L}_y = 0$ and $\sum \mathcal{F}_y = 0$ lead to the approximate solutions for the swimming speed and body rotation

$$
U_y \approx \frac{\mathcal{M}_{yy}^{F\Omega}}{\mathcal{M}_{yy}^{FU} + \mathcal{N}_{yy}^{FU}} \omega, \tag{14a}
$$

$$
\Omega_y \approx \frac{\mathcal{M}_{yy}^{LU} \mathcal{M}_{yy}^{F\Omega}}{\mathcal{N}_{yy}^{L\Omega}(\mathcal{M}_{yy}^{FU} + \mathcal{N}_{yy}^{FU})} \omega, \tag{14b}
$$

and $\Omega_y$ is indeed verified to be much smaller than $\omega$. We can then use $\sum \mathcal{F}_z = 0$ and obtain

$$
U_z = \frac{1}{\mathcal{N}_{zz}^{FU}}[\mathcal{M}_{zx}^{F\Omega} \Omega_x + \mathcal{M}_{zz}^{F\Omega} \Omega_z]. \tag{15}
$$

It follows, by substituting Eq. 15 into $\sum \mathcal{L}_z = 0$ and evaluating the leading-order contribution, that

$$
U_x = \frac{1}{\mathcal{M}_{zx}^{LU}}\left[\frac{\mathcal{M}_{zz}^{LU} \mathcal{M}_{zx}^{F\Omega}}{\mathcal{N}_{zz}^{FU}} \Omega_x - \mathcal{M}_{zz}^{L\Omega} \Omega_z - \mathcal{W}_{zy}^{L\Omega} \omega\right]. \tag{16}
$$

As a consequence, substituting Eqs. 15 and 16 into $\sum \mathcal{L}_x = 0$, using Eq. 14a and evaluating the leading-order term leads to

$$
\mathcal{M}_{xx}^{L\Omega} \Omega_x + \frac{\mathcal{M}_{zz}^{L\Omega} \mathcal{M}_{xx}^{LU}}{\mathcal{M}_{zx}^{LU}} \Omega_z + \frac{\mathcal{V}_{xy}^{LU} \mathcal{M}_{yy}^{F\Omega}}{\mathcal{M}_{yy}^{FU} + \mathcal{N}_{yy}^{FU}} \omega = 0. \tag{17}
$$

Finally, substituting Eqs. 14a, 14b, and 16 into $\sum \mathcal{F}_x = 0$ and keeping the leading-order terms leads to

$$
\mathcal{M}_{xx}^{F\Omega} \Omega_x + \left[\frac{\mathcal{M}_{zz}^{L\Omega}(\mathcal{M}_{xx}^{FU} + \mathcal{N}_{xx}^{FU})}{\mathcal{M}_{zx}^{LU}} - \mathcal{M}_{xz}^{F\Omega}\right]\Omega_z
$$
$$
+ \frac{\mathcal{W}_{zy}^{L\Omega}(\mathcal{M}_{xx}^{FU} + \mathcal{N}_{xx}^{FU})}{\mathcal{M}_{zx}^{LU}} \omega = 0. \tag{18}
$$

Solving the $2 \times 2$ linear systems of equations given by Eqs. 17 and 18, and keeping only the leading-order terms, leads to approximate formulae for the $x$ and $z$ components of the rotation rates as

$$\Omega_x \approx -\frac{\mathcal{V}_{xy}^{LU}\mathcal{M}_{yy}^{F\Omega}}{\mathcal{M}_{xx}^{L\Omega}(\mathcal{M}_{yy}^{FU}+\mathcal{N}_{yy}^{FU})}\omega, \tag{19a}$$

$$\Omega_z \approx -\frac{\mathcal{W}_{zy}^{L\Omega}}{\left(\mathcal{M}_{zz}^{L\Omega}-\frac{\mathcal{M}_{xz}^{F\Omega}\mathcal{M}_{zx}^{LU}}{\mathcal{M}_{xx}^{FU}+\mathcal{N}_{xx}^{FU}}\right)}\omega. \tag{19b}$$

Note that the denominator in the equation for $\Omega_z$, Eq. 19b, is dominated by $\mathcal{M}_{zz}^{L\Omega}$ but not by much, so we need to keep both terms to obtain correct orders of magnitude. These equations allow us to verify that, for *E. coli*, $\Omega_x$ is much smaller than $\Omega_y$ and $\Omega_z$ is of the same order as $\Omega_y$. Note also that we obtain $\Omega_z < 0$, which means that the bacteria is swimming to its right (clockwise trajectory viewed from above) and that $\Omega_x < 0$, so that the bacteria will also have the tendency to swim into the surface. Also, we observe that

$$\frac{a\Omega_x}{U_y} \approx \frac{a\mathcal{V}_{xy}^{LU}}{\mathcal{M}_{xx}^{L\Omega}} \approx \left(\frac{a}{L_\parallel}\right)^3 \ll 1, \tag{20}$$

so the timescale for reorientation of the bacteria perpendicular to the surface is much larger than the typical swimming timescale; the assumption that the bacteria is and remains parallel to the surface is therefore valid on a typical swimming timescale.

Now, substituting Eq. 19a and Eq. 19b into Eq. 15 and Eq. 16 and keeping leading-order terms leads to

$$U_z \approx -\frac{\mathcal{V}_{xy}^{LU}\mathcal{M}_{zx}^{F\Omega}\mathcal{M}_{yy}^{F\Omega}}{\mathcal{N}_{zz}^{FU}\mathcal{M}_{xx}^{L\Omega}(\mathcal{M}_{yy}^{FU}+\mathcal{N}_{yy}^{FU})}\omega, \tag{21a}$$

$$U_x \approx \frac{\mathcal{W}_{zy}^{L\Omega}}{\left(\frac{\mathcal{M}_{zz}^{L\Omega}(\mathcal{M}_{xx}^{FU}+\mathcal{N}_{xx}^{FU})}{\mathcal{M}_{xz}^{F\Omega}}-\mathcal{M}_{zx}^{LU}\right)}\omega, \tag{21b}$$

and we get that $U_x > 0$ and, more important, that $U_z < 0$. This result, together with the result that $\Omega_x < 0$, shows that hydrodynamic interactions vertically trap the cell close to the wall. Note that this trapping does not require cells to be nonspherical (8). Note also that

$$\frac{U_x}{U_y} \approx \frac{\mathcal{W}_{zy}^{L\Omega}(\mathcal{M}_{yy}^{FU}+\mathcal{N}_{yy}^{FU})}{\mathcal{M}_{yy}^{F\Omega}\left(\frac{\mathcal{M}_{zz}^{L\Omega}(\mathcal{M}_{xx}^{FU}+\mathcal{N}_{xx}^{FU})}{\mathcal{M}_{xz}^{F\Omega}}-\mathcal{M}_{zx}^{LU}\right)} \approx \frac{3}{\epsilon}\mathcal{J} \ll 1, \tag{22}$$

where $\epsilon = 2\pi b/\lambda$ and $\mathcal{J}$ is defined in Appendix A, and

$$\frac{U_z}{U_y} \approx \frac{\mathcal{V}_{xy}^{LU}\mathcal{M}_{zx}^{F\Omega}}{\mathcal{N}_{zz}^{FU}\mathcal{M}_{xx}^{L\Omega}} \ll \frac{h}{L_\parallel} \ll 1, \tag{23}$$

so the calculation assumptions are consistent.

We can finally evaluate the approximate solution for the radius of curvature of the circular trajectory. It is given by

$$\mathcal{R} = \frac{U}{|\Omega_z|} \approx \frac{U_y}{|\Omega_z|}$$
$$\approx \frac{\mathcal{M}_{zz}^{L\Omega}\mathcal{M}_{yy}^{F\Omega}}{\mathcal{W}_{zy}^{L\Omega}(\mathcal{M}_{yy}^{FU}+\mathcal{N}_{yy}^{FU})}\left(1-\frac{\mathcal{M}_{xz}^{F\Omega}\mathcal{M}_{zx}^{LU}}{\mathcal{M}_{zz}^{L\Omega}(\mathcal{M}_{xx}^{FU}+\mathcal{N}_{xx}^{FU})}\right), \tag{24}$$

which is very similar to that given by the simple physical picture in Eq. 4.

The results of the analytical model are summarized in Table 2. When we set $\mathcal{V} = \mathcal{W} = 0$, and assume that the previous approximations still hold, the results from Appendix B (swimming far from surface) are recovered.

## RESULTS OF THE MODEL AND COMPARISON WITH EXPERIMENTS

### Parameters of the model

The geometric characteristics of the flagellar helical bundles that we use are $\lambda = 2.5\ \mu$m, $L_\parallel = 7.5\ \mu$m (number $n = 3$ of wavelengths), and $b = 250$ nm (12,13,46). It is more difficult to estimate the appropriate radius of the bundle. Individual

TABLE 2  Summary of the results of the simplified model for *E. coli* swimming near a solid surface; the mobilities are calculated in Appendix A

$$U_x \approx \frac{\mathcal{W}_{zy}^{L\Omega}}{\left(\frac{\mathcal{M}_{zz}^{L\Omega}(\mathcal{M}_{xx}^{FU}+\mathcal{N}_{xx}^{FU})}{\mathcal{M}_{xz}^{F\Omega}}-\mathcal{M}_{zx}^{LU}\right)}\omega$$

$$U_y \approx \frac{\mathcal{M}_{yy}^{F\Omega}}{\mathcal{M}_{yy}^{FU}+\mathcal{N}_{yy}^{FU}}\omega$$

$$U_z \approx -\frac{\mathcal{V}_{xy}^{LU}\mathcal{M}_{zx}^{F\Omega}\mathcal{M}_{yy}^{F\Omega}}{\mathcal{N}_{zz}^{FU}\mathcal{M}_{xx}^{L\Omega}(\mathcal{M}_{yy}^{FU}+\mathcal{N}_{yy}^{FU})}\omega$$

$$\Omega_x \approx -\frac{\mathcal{V}_{xy}^{LU}\mathcal{M}_{yy}^{F\Omega}}{\mathcal{M}_{xx}^{L\Omega}(\mathcal{M}_{yy}^{FU}+\mathcal{N}_{yy}^{FU})}\omega$$

$$\Omega_y \approx \frac{\mathcal{M}_{yy}^{LU}\mathcal{M}_{yy}^{F\Omega}}{\mathcal{N}_{yy}^{L\Omega}(\mathcal{M}_{yy}^{FU}+\mathcal{N}_{yy}^{FU})}\omega$$

$$\Omega_z \approx -\frac{\mathcal{W}_{zy}^{L\Omega}}{\left(\mathcal{M}_{zz}^{L\Omega}-\frac{\mathcal{M}_{xz}^{F\Omega}\mathcal{M}_{zx}^{LU}}{\mathcal{M}_{xx}^{FU}+\mathcal{N}_{xx}^{FU}}\right)}\omega$$

$$\mathcal{R} \approx \frac{\mathcal{M}_{zz}^{L\Omega}\mathcal{M}_{yy}^{F\Omega}}{\mathcal{W}_{zy}^{L\Omega}(\mathcal{M}_{yy}^{FU}+\mathcal{N}_{yy}^{FU})}\left(1-\frac{\mathcal{M}_{xz}^{F\Omega}\mathcal{M}_{zx}^{LU}}{\mathcal{M}_{zz}^{L\Omega}(\mathcal{M}_{xx}^{FU}+\mathcal{N}_{xx}^{FU})}\right)$$

flagella have radius of ~12 nm (1,12) and there are between two and six flagella per bundle (four, on average). Results of RFT away from surfaces in Chwang et al. (38) show that appropriate velocities and rotation rates are obtained if $r$ is between 100 nm and 200 nm (46). However, the radius of a tight bundle of seven flagella is approximately $r \approx 20$ nm (13,46), and comparison between SBT calculations and Image Velocimetry experiments in Kim et al. (31) has shown that the flow generated by a two-filament bundle in steady state is the same as the flow generated by a single rigid helix with radius twice that of individual filaments. We chose in this article to use $r = 50$ nm as an intermediate value; the dependence of the results on the value of $r$ will be addressed below. For the cell radius $a$, we take the equivalent sphere radius $a$ that has the same viscous resistance as the prolate ellipsoid of measured cell dimensions translating along its axis of symmetry (28) (as explained above); the experimental values of $a$ vary from 0.81 to 1.16 $\mu$m. The only parameter in the model whose value is unknown is the gap thickness $h$. The minimum distance cells can swim from the surface is ~10 nm because of the protrusion of the flagellar hook from the cell body (personal communication, R.M. Ford). Values of $h$ have been measured to be 30–40 nm (8) . To compare the model with our experimental data, we will assume $h$ to be in the range from 10 to approximately 100 nm.

## Comparison experiments/models with a fixed gap thickness *h*

In this section, we fix the value of the gap thickness to be the same for all cells, so that the center of each cell is located at the same distance $d = h + w/2$ from the nearby surface. Despite the scatter in our experimental data, we find that the results of the two hydrodynamic models (numerical solution of Eq. 11 and analytical solution from Table 2) are com-

parable and are consistent with our experimental data, both for the radius of curvature of the trajectory, $\mathcal{R} \approx 15$ to 35 $\mu$m, and the swimming speed, $U = (U_x^2 + U_y^2)^{1/2} \approx 20$ to 25 $\mu$m/s; both set of values compare also favorably with past experimental results as described in the Introduction.

The results comparing experiment and theory are illustrated in Fig. 5. Results are displayed for two values of $h$, $h = 10$ nm (*top*) and $h = 60$ nm (*bottom*). In both cases, the values of the flagella rotation speeds, $\omega$, were chosen to lead to the best least-square fit of the measured cell velocities by the full hydrodynamic model; we obtain $\omega = 156$ Hz when $h = 10$ nm and $\omega = 127$ Hz when $h = 60$ nm. These values are consistent with the measurements of Vigeant et al. (8) and with typical values for the rotation rate of flagella in *E. coli* (2,11,12). The overall best-fit to the data by the full model with a constant $h$ is obtained for $h = 16$ nm and $\omega = 148$ Hz.

We now discuss the difference in trends between the models and the experimental data. The full hydrodynamic model predicts that the swimming speed, $U$, decreases with the cell size $a$, in agreement with our measurements. This result is a consequence of the increase of the viscous resistance with the cell size. However, the model predicts that, when the gap thickness $h$ is fixed, the radius of curvature, $\mathcal{R}$, should remain approximately constant, in contrast with the results of our experiments. Indeed, as the cell size increases, so does the distance between the helical flagella and the wall, so the rotation-inducing torque decreases, leading to a decrease in the rotation rate of the bacteria. In the range of parameters studied here, both the swimming velocity and the rotation rate decrease by approximately the same amount with an increase in $a$, leading to an approximately constant value for R. Since the experimental data display an increase of the radius of curvature with cell size, we will explore the possibility of a relationship between $h$ and $a$ below.
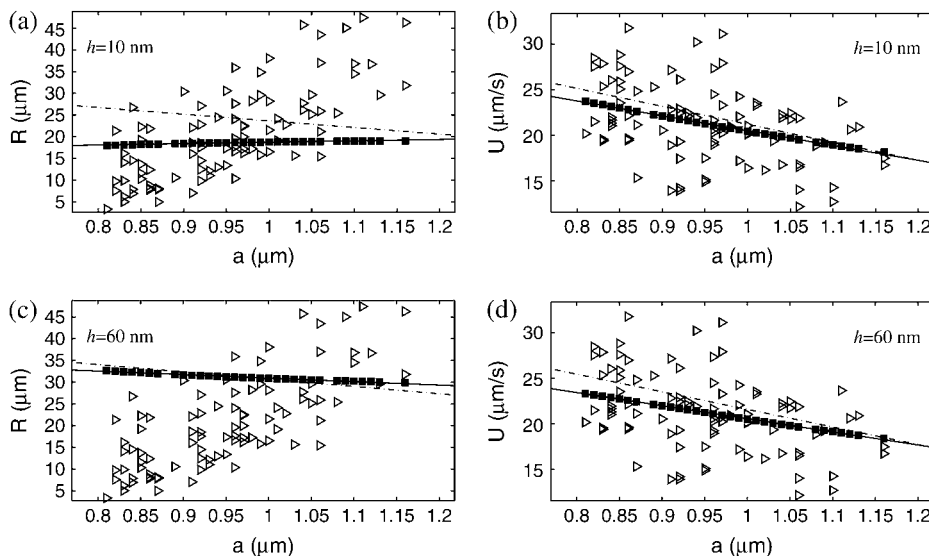


FIGURE 5  Comparison between the results of the experiments ($\triangleright$), the full hydrodynamic model (numerical solution of Eq. 11, $\blacksquare$; and best fit, *straight line*) and the simplified model (Table 2, *dash-dotted line*) with a fixed gap thickness *h*. (*Top*) $h = 10$ nm and $\omega = 156$ Hz: (*a*) radius of curvature, $\mathcal{R}$, and (*b*) swimming velocity, $U$, as a function of the bacterial radius $a$. (*Bottom*) $h = 60$ nm and $\omega = 127$ Hz: (*c*) radius of curvature, and (*d*) swimming velocity as a function of the bacteria radius $a$.

## Dependence of the models on the cell parameters

In the experimental data presented for *E. coli*, $\lambda$ and *b* should be approximately constant, but *a*, *r* (essentially proportional to the number of flagella), and $L_\parallel$, are likely to vary from cell to cell. We expect this variability to give rise to the scatter observed in the experimental data for $\mathcal{R}$ and *U*. In this section, we investigate the dependence of both the full model and the approximate analytical model on *r*, $L_\parallel$ (through *n*) to help explain the scatter observed in the experimental data, and we present the dependence of the model on $\lambda$ and *b* to help predict the behavior of organisms other than *E. coli*. (The dependence of the model on the cell body, *a*, and the gap thickness, *h*, are illustrated in Fig. 5. Moreover, from Eq.

11, it is straightforward to see that both **U** and **$\Omega$** scale with $\omega$, and therefore $\mathcal{R}$ is independent of $\omega$. Finally, since the viscous mobilities are all proportional to the viscosity of the liquid, $\mu$, both **U** and **$\Omega$**, solutions to Eq. 11, are independent of $\mu$, and therefore so is the radius of curvature $\mathcal{R}$.) To display the variations, we will fix the values to be $b = 250$ nm, $h = 30$ nm, $r = 50$ nm, $\lambda = 2.5$ $\mu$m, $L_\parallel = 3\lambda$ (that is, $n = 3$), and $\omega = 150$ Hz, and will then vary each one of the parameters $\{b, r, \lambda, n\}$ at a time. The results are displayed in Fig. 6 for the full hydrodynamic model (numerical solution of Eq. 11, *solid squares* and best fit, *solid lines*) and the approximate analytical model (Table 2, *dash-dotted lines*).

These results first confirm that both models are in agreement for the trends and values of the swimming velocity,
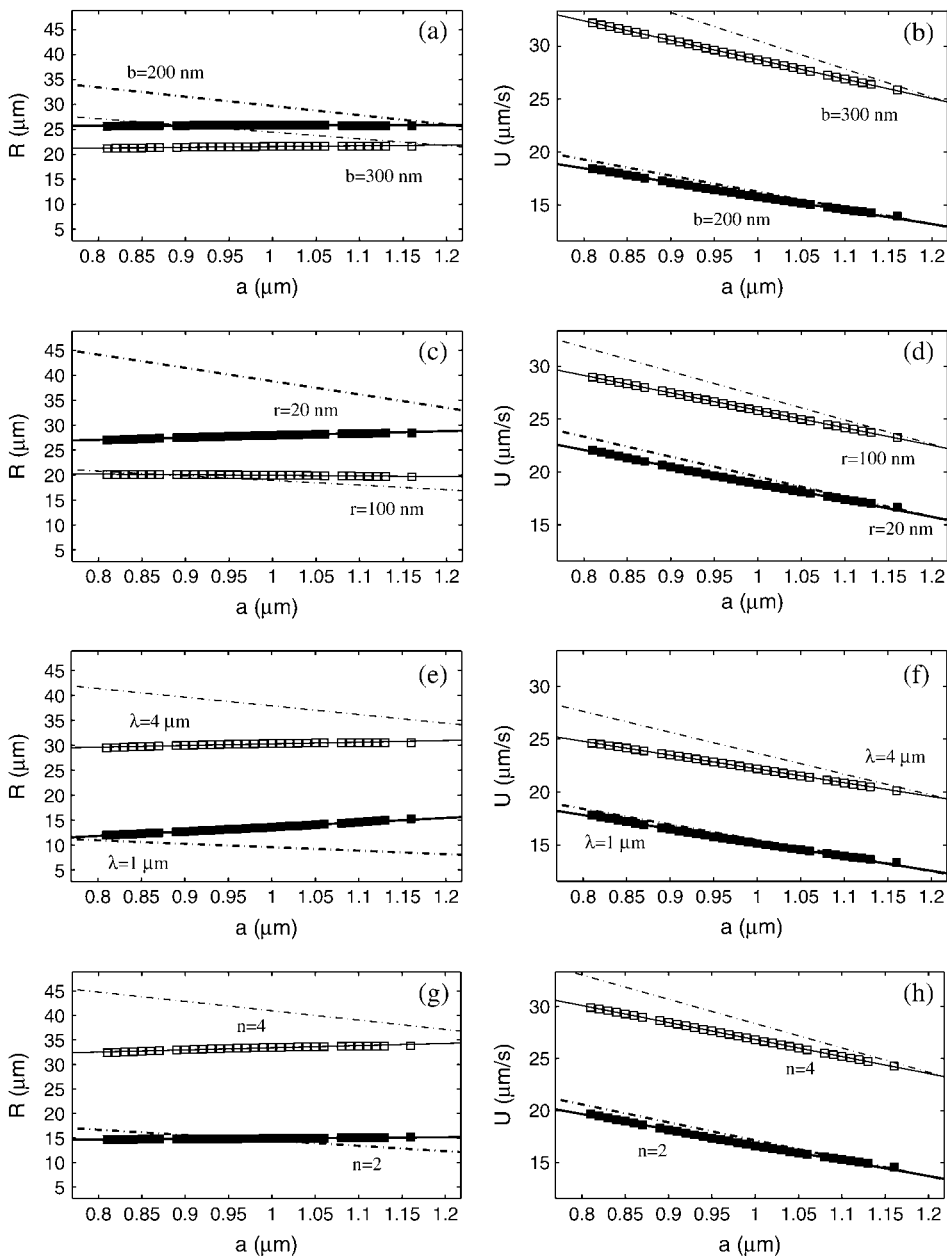


FIGURE 6 Dependence of the results $\{\mathcal{R}, U\}$ on the geometrical parameters $\{b, r, \lambda, n\}$ for the two models (full model: *squares* and best fit, *solid line*; approximate analytical model: *dash-dotted line*), in the case where $r = 50$ nm, $\lambda = 2.5$ $\mu$m, $b = 250$ nm, $L_\parallel = 3\lambda$ ($n = 3$), $h = 30$ nm, and $\omega = 150$ Hz, and one of the parameters is varied at a time. (*a* and *b*) Dependence on the helix radius, *b*, for two values: $b = 200$ nm (■ and *thick lines*) and $b = 300$ nm (□ and *regular lines*). (*c* and *d*) Dependence on the bundle radius, *r*, for two values: $r = 20$ nm (■ and *thick lines*) and $r = 100$ nm (□ and *regular lines*). (*e* and *f*) Dependence on the helix wavelength, $\lambda$, for two values: $\lambda = 1$ $\mu$m (■ and *thick lines*) and $\lambda = 4$ $\mu$m (□ and *regular lines*). (*g* and *h*) Dependence on the number of wavelengths, *n*, for two values: $n = 2$ (■ and *thick lines*) and $n = 4$ (□ and *regular lines*).

although the approximate analytical model can lead to large errors for the radius of curvature of the trajectory (by up to 50%). For both models, the dependence of the swimming velocity, $U$, on the four parameters is found to be consistent with the increase of the propulsive viscous force with $b, r, \lambda$, and $n$ (see the values of the mobilities as calculated in Appendix A). The radius of curvature decreases with $r$, consistent with an increase in the hydrodynamic interactions with the nearby surface as described by Eq. 7. Furthermore, $\mathcal{R}$ decreases with $b$, confirming the important role of the viscous resistance on parts of the helix that are close to the surface (whose distance to the surface decreases with $b$) in inducing the torque on the cell in the $z$-direction. Finally, the increase of $\mathcal{R}$ with $\lambda$ and $n$ probably follows that of $U$, through Eq. 12.

## Comparison experiments/models using a relationship between cell size and gap thickness

As was observed earlier, the value of the radius of curvature from the model depends strongly on the unknown gap thickness $h$. Returning to the comparison with the results of our experiments, we see that data for larger cells tend to be more consistent with the model for large values of $h$ (Figs. 5 and 6). Thus we propose here that, if we suppose that all bacteria have the same geometrical characteristics, $\{b, r, \lambda, L_{\parallel}\}$, our hydrodynamic model could be used to estimate the relation between the typical cell size, $a$, and its steady-state distance to the wall, $h$, by fitting the model to the experimental data of Fig. 2, which show an increase of $\mathcal{R}$ with cell size. The results are illustrated in Fig. 7, where we have plotted together the results of the experiments with two predictions of the full hydrodynamic model (Eq. 11) where the cell parameters are given above and where we assume a linear relationship between $a$ and $h$,

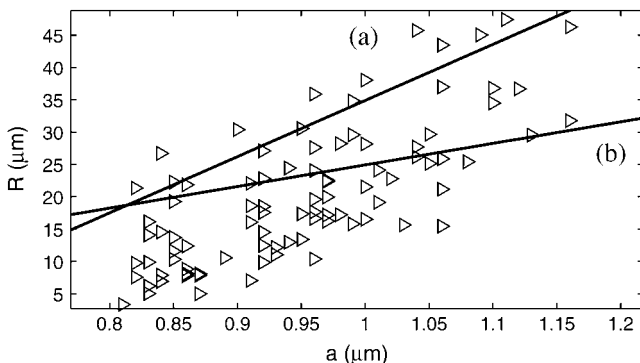$$h(a) = h_0 + \left(\frac{a - a_1}{a_2}\right) h_1. \tag{25}$$



FIGURE 7   Best fit to the experimental data ($\triangleright$) by an $h(a)$ law in the full hydrodynamic model (numerical solution of Eq. 11, *straight line*), as given by Eq. 25. The relation between $h$ and $a$ is chosen to obtain the same linear slope for the results of the model and the experimental data (*a*) and the best least-square difference between the model and the data (*b*).

The parameters for this fit are $h_0 = 10$ nm, $a_1 = 0.81$ $\mu$m, $a_2 = 0.35$ $\mu$m, and the value of $h_1$ is chosen to lead to the same correlation (slope) between the results of the model and the experimental data (a, $h_1 = 119$ nm) or the best possible least-square difference between the model and the data (b, $h_1 = 48$ nm).

## CONCLUSION

We have presented a hydrodynamic model for the swimming of *E. coli* near solid boundaries and compared it to a new set of measurements of cell velocities and trajectories. We have shown that force-free and torque-free swimming was responsible for the clockwise circular motion of the cells, $\Omega_z < 0$, as well as for their hydrodynamic vertical trapping close to the surface, that is, $\Omega_x < 0$ and $U_z < 0$. This trapping is probably responsible for the extended period of time during which cells are observed to remain near surfaces, which enhances the probability of cell adhesion to substrates. Determining the mechanisms responsible for the relationship between $h$ and $a$ we inferred from the measurements would be valuable.

The main assumptions made in this article, and which illustrate the differences between real swimming *E. coli* cells and our model, are the following:

1. We have replaced the bundle of several flagella by a single rigid helix; according to the results of Kim et al. (31), this might not be a large source of error.
2. We have assumed that the cell body was spherical; this assumption is probably more important, and an analysis using a nonspherical head might lead to an explanation of the increase of the distance to the wall, $h$, with the cell size.
3. We have ignored all interactions between the cell body and the flagella.
4. We have ignored Brownian motion.

Although relaxing these assumptions would improve on the agreement between theory and experiments, we do not expect it would change the physical picture given in this article for the circular motion. Including the presence of a second (top) boundary should also modify the cell trajectories (47). If the surface was a perfectly-slipping interface (such as the free surface between air and water) instead of a no-slip surface, the change of the direction of the image system for a point force (48) should lead to bacteria swimming in circles, but in a counterclockwise direction (X.L. Lu, University of Pittsburgh, private communication).

Finally, our experimental finding that the radius of curvature of cell trajectories depends on the size of the cell, suggests a new strategy for sorting cells by size using hydrodynamic interactions.

## APPENDIX A: CELL MOBILITIES

We present in this Appendix the values of the hydrodynamic mobilities of the bacteria. First, since we have $h \ll a$, the lubrication approximation can

be made to derive the mobilities for the cell body (41–44). We find that they are given by

$$\mathcal{N}_{xx}^{FU} = \mathcal{N}_{yy}^{FU} = 6\pi\mu a \left[\frac{8}{15}\ln\left(\frac{a}{h}\right) + 0.96\right], \qquad (26a)$$

$$\mathcal{N}_{zz}^{FU} = 6\pi\mu \frac{a^2}{h}, \qquad (26b)$$

$$\mathcal{N}_{xx}^{L\Omega} = \mathcal{N}_{yy}^{L\Omega} = 8\pi\mu a^3 \left[\frac{2}{5}\ln\left(\frac{a}{h}\right) + 0.38\right], \qquad (26c)$$

$$\mathcal{N}_{zz}^{L\Omega} = 8\pi\mu a^3, \qquad (26d)$$

$$\mathcal{V}_{xy}^{LU} = \mathcal{V}_{yx}^{LU} = 8\pi\mu a^2 \left[\frac{1}{10}\ln\left(\frac{a}{h}\right) - 0.19\right], \qquad (26e)$$

$$\mathcal{V}_{xy}^{F\Omega} = \mathcal{V}_{yx}^{F\Omega} = 6\pi\mu a^2 \left[\frac{2}{15}\ln\left(\frac{a}{h}\right) - 0.25\right]. \qquad (26f)$$

Note that we assumed that $\mathcal{N}_{zz}^{\prime L\Omega}$ was equal to its far-field value, as it was shown that the presence of a nearby surface has only a small effect on the value of this mobility (41).

Second, the bundle of helical flagella is described by the equation

$$\begin{cases} x = b\sin(s - \omega t) \\ y = -\dfrac{\lambda}{2\pi}(s + s_0) \\ z = b\cos(s - \omega t) \end{cases}, \qquad (27)$$

where $s$ ranges from 0 to $2n\pi$, and $\omega$ is the rotation rate of the flagella bundle relative to the cell body. In that case, the mobility calculation was done according to RFT and we get

$$\mathcal{M}_{xx}^{FU} = \mathcal{M}_{zz}^{FU} = 2\overline{c_\parallel} L_\parallel \frac{1 + 3\epsilon^2/4}{(1 + \epsilon^2)^{1/2}}, \qquad (28a)$$

$$\mathcal{M}_{yy}^{FU} = \overline{c_\parallel} L_\parallel \frac{1 + 2\epsilon^2}{(1 + \epsilon^2)^{1/2}}, \qquad (28b)$$

$$\mathcal{M}_{yy}^{LU} = \mathcal{M}_{yy}^{F\Omega} = \overline{c_\parallel} bL_\parallel \frac{\epsilon}{(1 + \epsilon^2)^{1/2}}, \qquad (28c)$$

$$\mathcal{M}_{xx}^{L\Omega} = \mathcal{M}_{zz}^{L\Omega} = \frac{2}{3}\overline{c_\parallel} L_\parallel^3 \frac{1 + 3\epsilon^2/4}{(1 + \epsilon^2)^{1/2}}, \qquad (28d)$$

$$\mathcal{M}_{zx}^{F\Omega} = \mathcal{M}_{xz}^{F\Omega} = \mathcal{M}_{xz}^{LU} = \mathcal{M}_{zx}^{LU} = \overline{c_\parallel} L_\parallel^2 \frac{1 + 3\epsilon^2/4}{(1 + \epsilon^2)^{1/2}}, \qquad (28e)$$

$$\mathcal{M}_{yy}^{L\Omega} = 2\overline{c_\parallel} b^2 L_\parallel \frac{1 + \epsilon^2/2}{(1 + \epsilon^2)^{1/2}}, \qquad (28f)$$

$$\mathcal{M}_{xx}^{LU} = \mathcal{M}_{zz}^{LU} = \mathcal{M}_{xx}^{F\Omega} = \mathcal{M}_{zz}^{F\Omega} = \frac{1}{2}\overline{c_\parallel} bL_\parallel \frac{\epsilon}{(1 + \epsilon^2)^{1/2}}, \qquad (28g)$$

$$\mathcal{W}_{yx}^{LU} = \mathcal{W}_{xy}^{F\Omega} = -2\overline{c_\parallel} bL_\parallel \frac{1 + \epsilon^2/2}{(1 + \epsilon^2)^{1/2}}\mathcal{I}, \qquad (28h)$$

$$\mathcal{W}_{xy}^{FU} = \mathcal{W}_{yx}^{FU} = -\overline{c_\parallel} L_\parallel \frac{\epsilon}{(1 + \epsilon^2)^{1/2}}\mathcal{I}, \qquad (28i)$$

$$\mathcal{W}_{zy}^{LU} = \mathcal{W}_{yz}^{F\Omega} = -\overline{c_\parallel} L_\parallel^2 \frac{\epsilon}{(1 + \epsilon^2)^{1/2}}\mathcal{J}, \qquad (28j)$$

$$\mathcal{W}_{xy}^{LU} = \mathcal{W}_{yx}^{F\Omega} = -\overline{c_\parallel} bL_\parallel \frac{1 + 2\epsilon^2}{(1 + \epsilon^2)^{1/2}}\mathcal{I}, \qquad (28k)$$

$$\mathcal{W}_{zy}^{L\Omega} = \mathcal{W}_{yz}^{L\Omega} = -2\overline{c_\parallel} bL_\parallel^2 \frac{1 + \epsilon^2/2}{(1 + \epsilon^2)^{1/2}}\mathcal{J}, \qquad (28l)$$

$$\mathcal{W}_{xy}^{L\Omega} = \mathcal{W}_{yx}^{L\Omega} = -\overline{c_\parallel} b^2 L_\parallel \frac{\epsilon}{(1 + \epsilon^2)^{1/2}}\mathcal{I}, \qquad (28m)$$

where $\epsilon = 2\pi b/\lambda$, and where we have defined the two integrals

$$\mathcal{I} = \int_0^1 \cos(2\pi u)f(\cos(2\pi u))du,$$

$$\mathcal{J} = \int_0^1 (u + u_0)\cos(2\pi nu)f(\cos(2\pi nu))du. \qquad (29)$$

Note that for the calculation of $\mathcal{M}_{yy}^{L\Omega}$, the contribution due to the local rotation of the flagella can be neglected because $r \ll b$ (38).

## APPENDIX B: SWIMMING FAR FROM A SURFACE

When the bacteria swims away from a surface, we have $\mathcal{W} = 0$ and $\mathcal{V} = 0$, so the mobility matrices become

$$\mathcal{A} = \begin{pmatrix} -\mathcal{N}_{xx}^{FU} & 0 & 0 & 0 & 0 & 0 \\ 0 & -\mathcal{N}_{yy}^{FU} & 0 & 0 & 0 & 0 \\ 0 & 0 & -\mathcal{N}_{zz}^{FU} & 0 & 0 & 0 \\ 0 & 0 & 0 & -\mathcal{N}_{xx}^{L\Omega} & 0 & 0 \\ 0 & 0 & 0 & 0 & -\mathcal{N}_{yy}^{L\Omega} & 0 \\ 0 & 0 & 0 & 0 & 0 & -\mathcal{N}_{zz}^{L\Omega} \end{pmatrix}, \qquad (30)$$

and

$$\mathcal{B} = \begin{pmatrix} -\mathcal{M}_{xx}^{FU} & 0 & 0 & \mathcal{M}_{xx}^{F\Omega} & 0 & -\mathcal{M}_{xz}^{F\Omega} \\ 0 & -\mathcal{M}_{yy}^{FU} & 0 & 0 & -\mathcal{M}_{yy}^{F\Omega} & 0 \\ 0 & 0 & -\mathcal{M}_{zz}^{FU} & \mathcal{M}_{zx}^{F\Omega} & 0 & \mathcal{M}_{zz}^{F\Omega} \\ \mathcal{M}_{xx}^{LU} & 0 & \mathcal{M}_{xz}^{LU} & -\mathcal{M}_{xx}^{L\Omega} & 0 & 0 \\ 0 & \mathcal{M}_{yy}^{LU} & 0 & 0 & -\mathcal{M}_{yy}^{L\Omega} & 0 \\ -\mathcal{M}_{zx}^{LU} & 0 & \mathcal{M}_{zz}^{LU} & 0 & 0 & -\mathcal{M}_{zz}^{L\Omega} \end{pmatrix}. \qquad (31)$$

Solving Eq. 11 for the velocities and rotation rates in this case leads to $U_x = U_z = \Omega_x = \Omega_z = 0$ and

$$U_y = \frac{\mathcal{M}_{yy}^{F\Omega}\mathcal{N}_{yy}^{L\Omega}}{(\mathcal{M}_{yy}^{L\Omega} + \mathcal{N}_{yy}^{L\Omega})(\mathcal{M}_{yy}^{FU} + \mathcal{N}_{yy}^{FU}) + \mathcal{M}_{yy}^{F\Omega}\mathcal{M}_{yy}^{LU}}\omega, \qquad (32a)$$

$$\Omega_y = \frac{\mathcal{M}_{yy}^{L\Omega}(\mathcal{M}_{yy}^{FU} + \mathcal{N}_{yy}^{FU}) + \mathcal{M}_{yy}^{F\Omega}\mathcal{M}_{yy}^{LU}}{(\mathcal{M}_{yy}^{L\Omega} + \mathcal{N}_{yy}^{L\Omega})(\mathcal{M}_{yy}^{FU} + \mathcal{N}_{yy}^{FU}) + \mathcal{M}_{yy}^{F\Omega}\mathcal{M}_{yy}^{LU}}\omega. \qquad (32b)$$

In the absence of a wall, the bacteria swims therefore in a straight line and rotates its body in the direction opposed to that of the flagella.

## REFERENCES

1. Berg, H. C. 2000. Motile behavior of bacteria. *Phys. Today*. 53:24–29.

2. Berg, H. C. 2004. *Escherichia coli* in Motion. Springer-Verlag, New York.

3. Maeda, K., Y. Imae, J. I. Shioi, and F. Oosawa. 1976. Effect of temperature on motility and chemotaxis of *Escherichia coli*. *J. Bacteriol.* 127:1039–1046.

4. Berg, H. C., and L. Turner. 1990. Chemotaxis of bacteria in glass capillary arrays—*Escherichia coli*, motility, microchannel plate, and light scattering. *Biophys. J.* 58:919–930.

5. Frymier, P. D., R. M. Ford, H. C. Berg, and P. T. Cummings. 1995. Three-dimensional tracking of motile bacteria near a solid planar surface. *Proc. Natl. Acad. Sci. USA*. 92:6195–6199.

6. Frymier, P. D., and R. M. Ford. 1997. Analysis of bacterial swimming speed approaching a solid-liquid interface. *AIChE J.* 43:1341–1347.

7. Vigeant, M. A. S., and R. M. Ford. 1997. Interactions between motile *Escherichia coli* and glass in media with various ionic strengths, as observed with a three-dimensional tracking microscope. *Appl. Environ. Microbiol.* 63:3474–3479.

8. Vigeant, M. A. S., R. M. Ford, M. Wagner, and L. K. Tamm. 2002. Reversible and irreversible adhesion of motile *Escherichia coli* cells analyzed by total internal reflection aqueous fluorescence microscopy. *Appl. Environ. Microbiol.* 68:2794–2801.

9. Ottemann, K. M., and J. F. Miller. 1997. Roles for motility in bacterial-host interactions. *Mol. Microbiol.* 24:1109–1117.

10. Pratt, L. A., and R. Kolter. 1998. Genetic analysis of *Escherichia coli* biofilm formation: roles of flagella, motility, chemotaxis and Type I pili. *Mol. Microbiol.* 30:285–293.

11. Lowe, G., M. Meister, and H. C. Berg. 1987. Rapid rotation of flagellar bundles in swimming bacteria. *Nature*. 325:637–640.

12. Magariyama, Y., S. Sugiyama, and S. Kudo. 2001. Bacterial swimming speed and rotation rate of bundled flagella. *FEMS Microbiol. Lett.* 199:125–129.

13. Macnab, R. M. 1977. Bacterial flagella rotating in bundles—study in helical geometry. *Proc. Natl. Acad. Sci. USA*. 74:221–225.

14. Kudo, S., N. Imai, M. Nishitoba, S. Sugiyama, and Y. Magariyama. 2005. Asymmetric swimming pattern of *Vibrio alginolyticus* cells with single polar flagella. *FEMS Microbiol. Lett.* 242:221–225.

15. Magariyama, Y., M. Ichiba, K. Nakata, K. Baba, T. Ohtani, S. Kudo, and T. Goto. 2005. Difference in bacterial motion between forward and backward swimming caused by the wall effect. *Biophys. J.* 88:3648–3658.

16. Ramia, M., D. L. Tullock, and N. Phan-Thien. 1993. The role of hydrodynamic interaction in the locomotion of microorganisms. *Biophys. J.* 65:755–778.

17. Reynolds, A. J. 1965. Swimming of minute organisms. *J. Fluid Mech.* 23:241–260.

18. Katz, D. F. 1974. Propulsion of microorganisms near solid boundaries. *J. Fluid Mech.* 64:33–49.

19. Katz, D. F., J. R. Blake, and S. L. Paverifontana. 1975. Movement of slender bodies near plane boundaries at low Reynolds-number. *J. Fluid Mech.* 72:529–540.

20. Katz, D. F., and J. R. Blake. 1975. Flagellar motions near walls. *In* Swimming and Flying in Nature, Vol. 1. T.Y. Wu, C.J. Brokaw, and C Brennen, editors. Plenum Press, New York. 173–184.

21. Brennen, C., and H. Winet. 1977. Fluid mechanics of propulsion by cilia and flagella. *Annu. Rev. Fluid Mech.* 9:339–398.

22. Wolfe, A. J., M. P. Conley, T. J. Kramer, and H. C. Berg. 1987. Reconstitution of signaling in bacterial chemotaxis. *J. Bacteriol.* 169:1878–1885.

23. Neidhardt, F. C., R. Curtiss III, J. L. Ingraham, E. C. C. Lin, K. B. Low, B. Magasanik, W. S. Reznikoff, M. Riley, M. Schaechter, and H. E. Umbarger (editors). 1996. Growth of cells and cultures. *In Escherichia coli* and *Salmonella*: Cellular and Molecular Biology, 2nd Ed. ASM Press, Washington, DC.

24. Adler, J., and B. Templeton. 1967. Effect of environmental conditions on motility of *Escherichia coli*. *J. Gen. Microbiol.* 46:175–184.

25. Berg, H. C., and D. A. Brown. 1972. Chemotaxis in *Escherichia coli* analyzed by three-dimensional tracking. *Nature*. 239:500–504.

26. Berg, H. C., and L. Turner. 1979. Movement of microorganisms in viscous environments. *Nature*. 278:349–351.

27. Maki, N., J. E. Gestwicki, E. M. Lake, L. L. Kiessling, and J. Adler. 2000. Motility and chemotaxis of filamentous cells of *Escherichia coli*. *J. Bacteriol.* 182:4337–4342.

28. Happel, J., and H. Brenner. 1965. Low Reynolds Number Hydrodynamics. Prentice Hall, Englewood Cliffs, NJ.

29. Turner, L., W. S. Ryu, and H. C. Berg. 2000. Real-time imaging of fluorescent flagellar filaments. *J. Bacteriol.* 182:2793–2801.

30. Higdon, J. J. L. 1979. Hydrodynamics of flagellar propulsion—helical waves. *J. Fluid Mech.* 94:331–351.

31. Kim, M. J., M. M. J. Kim, J. C. Bird, J. Park, T. R. Powers, and K. S. Breuer. 2004. Particle image velocimetry experiments on a macro-scale model for bacterial flagellar bundling. *Exp. Fluids*. 37:782–788.

32. Yates, G. T. 1986. How microorganisms move through water. *Am. Sci.* 74:358–365.

33. Cox, R. G. 1970. The motion of long slender bodies in a viscous fluid. Part 1. General theory. *J. Fluid Mech.* 44:791–810.

34. Gray, J., and G. J. Hancock. 1955. The propulsion of sea-urchin spermatozoa. *J. Exp. Biol.* 32:802–814.

35. Keller, J. B., and S. I. Rubinow. 1976. Slender-body theory for slow viscous flow. *J. Fluid Mech.* 75:705–714.

36. Hancock, G. J. 1953. The self-propulsion of microscopic organisms through liquids. *Proc. R. Soc. Lond. A*. 217:96–121.

37. Lighthill, J. 1976. Flagellar hydrodynamics—the John von Neumann lecture, 1975. *SIAM Rev.* 18:161–230.

38. Chwang, A. T., and T. Y. Wu. 1971. Helical movement of microorganisms. *Proc. R. Soc. Lond. B Biol. Sci.* 178:327–346.

39. Childress, S. 1981. Mechanics of Swimming and Flying. Cambridge University Press, Cambridge, UK.

40. Wiggins, C. H., and R. E. Goldstein. 1928. Flexive and propulsive dynamics of elastica at low Reynolds number. *Phys. Rev. Lett.* 80:3879–3882.

41. Jeffrey, G. B. 1915. On the steady rotation of a solid of revolution in a viscous fluid. *Proc. Lond. Math. Soc.* 2:327–338.

42. Goldman, A. J., R. G. Cox, and H. Brenner. 1967. Slow viscous motion of a sphere parallel to a plane wall. I. Motion through a quiescent fluid. *Chem. Eng. Sci.* 22:637–651.

43. O'Neill, M. E., and K. Stewartson. 1967. On slow motion of a sphere parallel to a nearby plane wall. *J. Fluid Mech.* 27:705–724.

44. Cooley, M. D. A., and M. E. O'Neill. 1968. On the slow rotation of a sphere about a diameter parallel to a nearby plane wall. *J. Inst. Math. Appl.* 4:163–173.

45. Jeffrey, D. J., and Y. Onishi. 1981. The slow motion of a cylinder next to a plane wall. *Quart. J. Mech. Appl. Math.* 34:129–137.

46. Anderson, R. A. 1975. Formation of the bacterial flagellar bundle. *In* Swimming and Flying in Nature, Vol. 1. T.Y. Wu, C.J. Brokaw, and C. Brennen, editors. Plenum Press, New York. 45–56.

47. DiLuzio, W. R., L. Turner, M. Mayer, P. Garstecki, D. B. Weibel, H. C. Berg, and G. M. Whitesides. 2005. *Escherichia coli* swim on the right-hand side. *Nature*. 435:1271–1274.

48. Blake, J. R. 1971. A note on the image system for a Stokeslet in a no-slip boundary. *Proc. Camb. Phil. Soc.* 70:303–310.